molecular pharmaceutics

pubs.acs.org/molecularpharmaceutics

Article

Biodistribution and Activity of EGFR Targeted Polymeric Micelles Delivering a New Inhibitor of DNA Repair to Orthotopic Colorectal Cancer Xenografts with Metastasis

Igor Moura de Paiva, Mohammad Reza Vakili, Amir Hasan Soleimani, Seyed Amirhossein Tabatabaei Dakhili, Sirazum Munira, Marco Paladino, Gary Martin, Frank R. Jirik, Dennis G. Hall, Michael Weinfeld, and Afsaneh Lavasanifar*

Cite This: *Mol. Pharmaceutics* 2022, 19, 1825−1838

Read Online

ACCESS | Metrics & More | Article Recommendations | Supporting Information

ABSTRACT: The disruption of polynucleotide kinase/phosphatase (PNKP) in colorectal cancer (CRC) cells deficient in phosphatase and tensin homolog (PTEN) is expected to lead to the loss of cell viability by a process known as synthetic lethality. In previous studies, we have reported on the encapsulation of a novel inhibitor of PNKP, namely, A83B4C63, in polymeric micelles and its activity in slowing the growth of PTEN-deficient CRC cells as well as subcutaneous xenografts. In this study, to enhance drug delivery and specificity to CRC tumors, the surface of polymeric micelles carrying A83B4C63 was modified with GE11, a peptide targeting epidermal growth factor receptor (EGFR) overexpressed in about 70% of CRC tumors. Using molecular dynamics (MD) simulations, we assessed the binding site and affinity of GE11 for EGFR. The GE11-modified micelles, tagged with a near-infrared fluorophore, showed enhanced internalization by EGFR-overexpressing CRC cells *in vitro* and a trend toward increased primary tumor homing in an orthotopic CRC xenograft *in vivo*. In line with these observations, the GE11 modification of polymeric micelles was shown to positively contribute to the improved therapeutic activity of encapsulated A83B4C63 against HCT116-PTEN$^{-/-}$ cells *in vitro* and that of orthotopic CRC xenograft *in vivo*. In conclusion, our results provided proof of principle evidence for the potential benefit of EGFR targeted polymeric micellar formulations of A83B4C63 as monotherapeutics for aggressive and metastatic CRC tumors but at the same time highlighted the need for the development of EGFR ligands with improved physiological stability and EGFR binding.

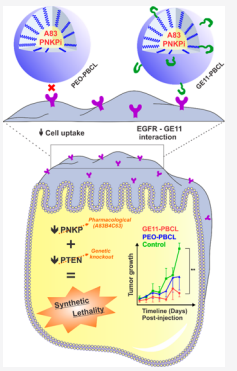

KEYWORDS: *colon cancer, polymeric micelles, drug delivery, GE11 peptide, mice imaging*

INTRODUCTION

Colorectal cancer (CRC) is the third most common cause of cancer mortality worldwide affecting 1.8 million people annually.[1,2] Surgical resection remains the first line of treatment, which may be complemented mostly by chemotherapy.[3,4] Common regimens for the management of CRC include 5-fluorouracil (5-FU), irinotecan, oxaliplatin, as well as their combinations, such as FOLFOX (leucovorin, 5-FU, and oxaliplatin), FOLFIRI (leucovorin, 5-FU, and irinotecan), and XELOX (oxaliplatin and capecitabine). Nevertheless, over 60% of CRC patients will eventually relapse or develop *de novo* metastatic disease.[5] More recently, CRC therapeutic strategies have made use of inhibitors of epidermal growth factor receptor (EGFR), either as a monotherapy or in combination with standard cytotoxic agents. EGFR is known to be overexpressed in 60−80% of CRC cases in patients.[6] These regimens are usually used to control unresectable tumor growth and its further spread or to reduce the size of locally metastasized cancer making the patient a candidate for surgery and tumor removal at metastatic sites. Chemotherapeutics used in metastatic CRC (mCRC) display indiscriminate toxicity when administered systemically and are not curative. Even with these treatments, the median overall survival in mCRC is approximately 30 months, highlighting the need for the development of new treatments.[7−10]

DNA repair enzymes have recently emerged as therapeutic targets in cancer. This is partly due to the success of inhibitors of poly(ADP-ribose) polymerase (PARP) in the treatment of many solid tumors including CRC.[11,12] Our research team has been studying another DNA repair enzyme, i.e., human polynucleotide kinase/phosphatase (PNKP), as a potential therapeutic target in CRC. This enzyme plays a key role in both single- and double-strand break repair, and its inhibition can make cancer cells sensitive to DNA damage by ionizing radiation (IR) as well as topoisomerase I inhibitors.[13] Through RNAi screens, we have also made an exciting discovery that deficiency in a tumor suppressor protein, i.e., phosphatase and

Special Issue: Tiny Things, Huge Impact: Nanomedicine in Canada

Received: December 1, 2021
Revised: February 23, 2022
Accepted: February 25, 2022
Published: March 10, 2022

https://doi.org/10.1021/acs.molpharmaceut.1c00918
Mol. Pharmaceutics 2022, 19, 1825−1838

tensin homolog (PTEN), makes cancer cells even more sensitive to PNKP inhibition.[14] These findings inspired the development of two generations of small molecular inhibitors of PNKP by our team.[13,15]

DNA repair inhibitors render tumors more susceptible to DNA damage but may act similarly on normal cells leading to intolerable toxicities in patients. Long circulating nanoparticles are known to have a capacity for passive accumulation in solid tumors through the enhanced permeation and retention (EPR) effect. To target CRC tumors, we have developed a polymeric micellar formulation of a lead PNKP inhibitor, namely, A83B4C63. In previous studies, the polymeric micellar formulation of A83B4C63 was shown to significantly enhance the delivery and activity of the incorporated drug in $PTEN^{-/-}$ HCT116 ectopic mouse xenografts.[16] This nanoformulation also sensitized wild-type $PTEN^{+/+}$ HCT116 xenografts to IR in a subcutaneous CRC mouse model.[17] We pursued modification of the surface of polymeric micellar carriers of A83B4C63 with a peptide ligand specific to EGFR, i.e., GE11. Specific delivery of PNKP inhibitors to PTEN-deficient CRC cells using EGFR targeted nanoparticles is expected to provide two simultaneous strategies for selectivity of these toxic compounds to aggressive $EGFR^+$ and $PTEN^-$ cancer cells over normal cells that are $EGFR^-$ and $PTEN^+$. In our previous study, GE11 modification of polymeric micelles was shown to increase their homing on EGFR positive subcutaneous tumors 24 h following iv administration using PET imaging for biodistribution assessments. The effect of this modification on homing of polymeric micelles in orthotopic and metastatic CRC lesions that mimic the actual location of CRC tumors was not known, however.[18] Here, for the first time, the effect of GE11 modification on homing of polymeric micelles in an orthotopic CRC model with metastasis to different organs was evaluated. Finally, the effect of GE11 modification of micellar carriers of A83B4C63 on the growth of orthotopic and mCRC tumors with PTEN deficiency was assessed.

Modification of nanoparticles using ligands specific for EGFR has been exploited mainly to enhance their homing/retention in the tumor site and/or increase nanocarrier cancer cell internalization in tumors that overexpress this receptor.[19−22] The dodecapeptide GE11 (YHWYGYTPQNVI) was originally identified, in 2005, for its EGFR affinity by phage display screening against the purified receptor.[23] Peptides are, in general, considered advantageous over other targeting ligands for surface modification of nanocarrier because they can be easily synthesized and further engineered for target specificity and/or stability against degradation in biological fluids. Peptide binding to the target protein/receptor usually does not require the formation of tertiary structures, as observed with full-length antibodies, single-chain variable fragments, diabodies, nanobodies, and other derivatives.[19,24,25] Also, their low immunogenicity makes short peptides a very attractive alternative for targeting receptors on cancer cells when compared to their high molecular weight protein based counterparts.[26]

GE11 has been explored as an EGFR internalizing ligand for the surface-modification of different nanoparticles carrying nucleic acids,[23,27,28] small molecule drugs,[28−30] photodynamic agents,[31] and radionuclides.[18] Interaction between GE11-modified nanoparticles and EGFR-expressing cells was shown to change the receptor level on the cell membrane minimally and not to activate the receptor dimerization and signaling. The latter is paramount for cancer targeting activity of an EGFR ligand since a low mitogenic activity is desired in order to avoid cell proliferation by the ligand.[27]

MATERIALS AND METHODS

Materials. Methoxy poly(ethylene oxide) (PEO, 5 kDa), ethylene oxide (≥99.9%), 3,3-diethoxy propanol, ascorbic acid, fetal bovine serum (FBS), and phenylmethylsulfonyl fluoride (PMSF) were purchased from Sigma (St. Louis, MO, USA). ε-Caprolactone (CL) was acquired from Lancaster Synthesis (Lancashire, England) and extra purified in-house by vacuum distillation. Two α-carbon modified-ε-caprolactone monomers (i.e., α-benzyl carboxylate-ε-caprolactone, BCL, and α-propargyl carboxylate-ε-caprolactone, PC) synthesized based on previously published methods[32,33] were obtained from Alberta Research Chemicals Inc. (Edmonton, Canada). Stannous octoate was purchased from MP Biomedicals Inc. (Tuttlingen, Germany) and further purified by vacuum distillation. Copper(II)-TBTA complex and Cy5.5-azide were acquired from Lumiprobe (Hallandale Beach, FL, USA). Cell culture media DMEM, DMEM:F12, sodium pyruvate, L-glutamine, nonessential amino acids, and penicillin−streptomycin were purchased from GIBCO Life Technologies (Burlington, ON, Canada). Protease and phosphatase inhibitor cocktails (no. 535140 and no. 524625, respectively) were from Millipore (Burlington, MA, USA). Antibody against EGFR (no. ab52894) was obtained from Abcam Inc. (Toronto, ON, Canada), and anti-β-actin (no. cst-4970) and horseradish peroxidase-conjugated anti-rabbit antibody were from Cell Signaling Technology (Danvers, MA, USA). Bicinchoninic acid (BCA) protein assay kit and Pierce ECL Western blotting substrate (no. 32106) were purchased from ThermoScientific (Rockford, IL, USA). The PNKP inhibitor, A83B4C63, was synthesized by Dr. Marco Paladino (Faculty of Science, Chemistry Department, University of Alberta). Peptide GE11 (YHWYGYTPQNVI) was acquired from Biomatik LLC (Wilmington, DE, USA). XenoLight D-luciferin potassium salt bioluminescent substrate was purchased from PerkinElmer (Waltham, MA, USA). The mouse food was the 2014S Teklad Global 14% protein rodent maintenance diet, from Harlan Labs (Indianapolis, IN, USA). Dialysis tubing (MWCO, 3.5 kDa) was purchased from Spectrum Laboratories (Rancho Dominguez, CA, USA). Toluene from Caledon (Halton Hills, ON, Canada) was dried by refluxing under H_2SO_4 before use. All other chemicals were reagent grade.

Synthesis of Heterobifunctional Polyethylene Oxide. Synthesis of acetal-polyethylene oxide (acPEO, Mn ∼ 5000) was performed based on the method described by Nagasaki et al.[34] with some modifications. Briefly, potassium naphthalene, used as a catalyst, was freshly prepared before the polymerization. Pure naphthalene (12.9 mmol) and potassium (14.7 mmol) were added into 50 mL of anhydrous THF. The reaction was protected under argon gas and kept running for 24 h. Then, 3,3-diethoxypropanol (2 mmol) was dissolved in 40 mL of dry THF, and 7 mL of the prepared catalyst (∼2 mmol) was added dropwise into the reaction solution to activate the initiator. The flask was purged with argon, and after 10 min of stirring, the flask was transferred into an ice water bath. Ethylene oxide (228 mmol) was added to the reaction solution. After 48 h, the polymerization was quenched by acidified ethanol. acPEO was recovered by precipitation in ethyl ether. The product was further purified by precipitation in diethyl ether. The composition and the degree of polymerization were confirmed by ^{1}H NMR (Bruker Advance

https://doi.org/10.1021/acs.molpharmaceut.1c00918
Mol. Pharmaceutics 2022, 19, 1825−1838

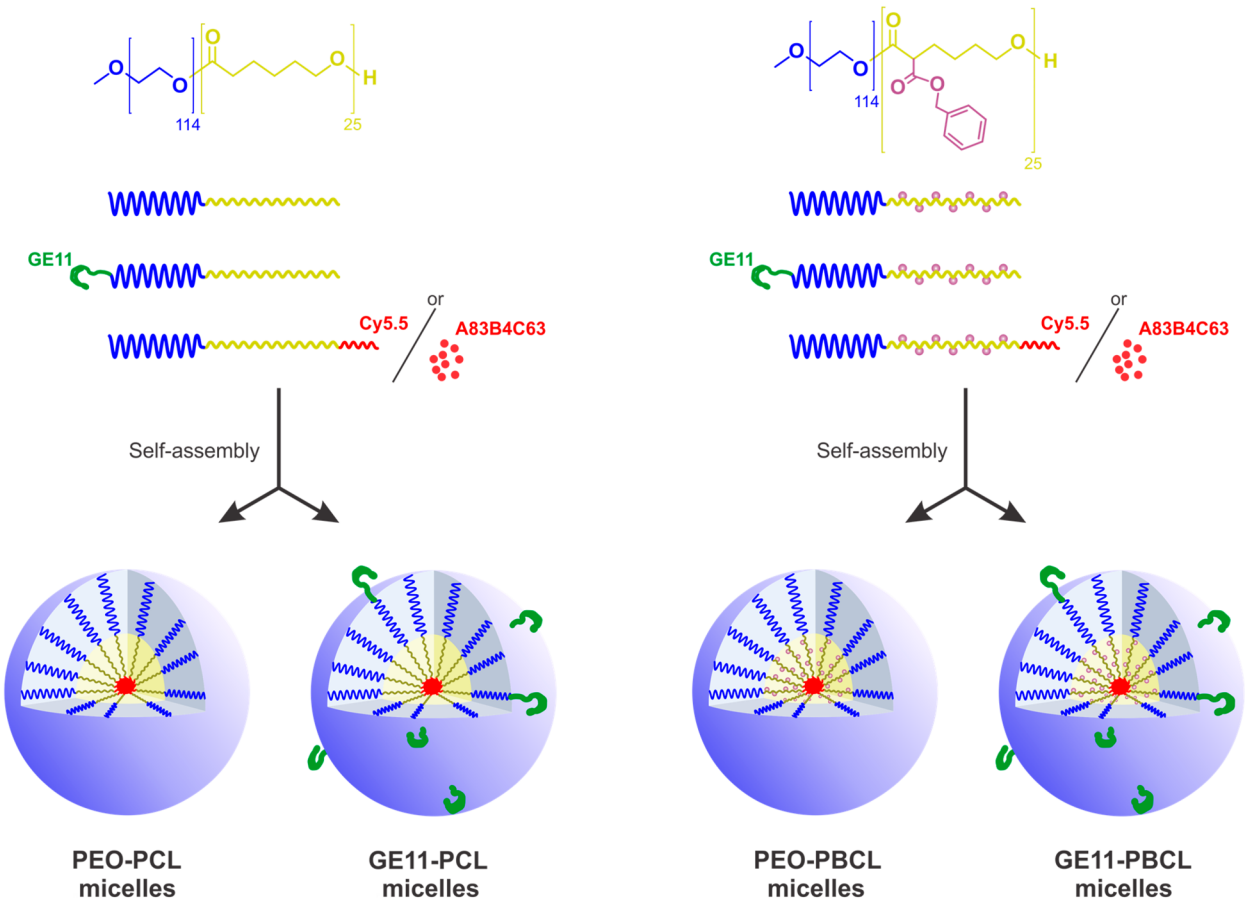

Figure 1. Model for the preparation of GE11-modified mixed micelles either tagged with Cy5.5 or physically loaded with A83B4C63 compound.

III 600 MHz Spectrometer, Bruker Corporation, Billerica, MA).

Synthesis of Peptide-Conjugated Polymers. The end hydroxyl group from synthesized acPEO was used to initiate the synthesis of the acPEO-*block*-ε-caprolactone, acPEO-*b*-PCL, and acPEO-*block*-(α-benzyl carboxylate-ε-caprolactone), acPEO-*b*-PBCL, which was carried out by bulk ring-opening polymerization of ε-caprolactone or BCL, respectively.[33] For peptide conjugation, micelles were prepared, by cosolvent evaporation, at a block copolymer concentration of 5 mg/mL. The pH was then adjusted to 2.0 using HCl (0.5 M solution). Micelles were then incubated at room temperature under stirring. After 2 h, the pH was readjusted to 7.4 with NaOH, followed by buffering of the micellar solution using PBS (10×, pH 7.4). An aqueous peptide solution in 1% DMSO was prepared and added, under constant stirring, at a peptide:polymer ratio (mol/mol) of 1:3. After 2 h reaction, $NaBH_3CN$ was added, and the reaction was left for 24 h at room temperature under constant stirring. The resulting micellar solution was extensively dialyzed against distilled water and lyophilized. The molar conjugation percent of GE11 peptide into the copolymers was determined by reverse-phase HPLC measuring unreacted peptide concentration (Varian Prostar 210 system, Microsorb-MV 5 μm C18 100 Å column, a gradient of 0.1% trifluoroacetic acid/acetonitrile).[35]

Synthesis of Three-Block Copolymers for Cy5.5 Conjugation. The PEO-*b*-PCL and PEO-*b*-PBCL diblock copolymers were used as the macroinitiator for the ring-opening polymerization of α-propargyl carboxylate-ε-caprolactone monomer as reported before to obtain poly(α-propargyl carboxylate-ε-caprolactone), i.e., PPC.[33] The copolymers were added together with PC in a 25 mL round-bottom flask previously filled with 5 mL of dry toluene under constant stirring. Stannous octoate was added to the flask and refluxed for 30 h. The reaction was stopped by cooling the system to room temperature. Both products, PEO-*b*-PCL-*b*-PPC and PEO-*b*-PBCL-*b*-PPC, were then precipitated in hexane, and the supernatant was discarded. Lastly, the copolymers were dissolved in THF and further purified with ether followed by drying under vacuum.

The near-infrared (NIR) dye Cy5.5, having an azide group (Cy5.5-azide), was conjugated to both triblock copolymers through azide−alkyne click chemistry.[36] Briefly, the pendant alkyne of PPC reacted with Cy5.5-azide, using Cu(I) as the catalyst. The triblock copolymers were dissolved in degassed DMSO. Also, Cy5.5-azide, ascorbic acid, and Cu(II) TBTA complex were added to the mixture under constant stirring. The reaction was performed at room temperature under argon for 16 h in the dark. After incubation, the mixture was separated from the nonreacted dye by dialysis against DMSO for 24 h followed by dialysis against water for 24 h and lyophilization. The conjugation efficiency of Cy5.5-azide to the copolymers was determined by fluorescence spectroscopy using a Synergy H1 hybrid multimode microplate reader (BioTek), measuring the excitation at 673 nm and emission at 707 nm.

Characterization of Synthesized Block Copolymers. The polymer synthesis reaction was assessed by nuclear

https://doi.org/10.1021/acs.molpharmaceut.1c00918
Mol. Pharmaceutics 2022, 19, 1825−1838

magnetic resonance (NMR) techniques and size exclusion chromatography (SEC). The number molecular weight (Mn) of diblock copolymers was determined using ^{1}H NMR by comparing the integration from methylene hydrogen signals of PCL or PBCL segments ($-OCH_2-$, δ = 4.05 ppm) to the ones from the PEO segment ($-CH_2CH_2O-$, δ = 3.65 ppm). In order to estimate the degree of polymerization of PPC, the area under the curve from PPC ($-OCH_2-$, δ = 4.75 ppm) was compared to that of the methylene hydrogens from PEO ($-CH_2CH_2O-$, δ = 3.65 ppm). The ^{1}H diffusion ordered NMR spectroscopy (DOSY) spectra were also recorded. Samples were dissolved in deuterated chloroform and then transferred to thin glass walled tubes for both types of NMR analyses, which were carried out using a Bruker 600 MHz spectrometer. For size exclusion chromatography (SEC), samples were dissolved in THF (~10 mg/mL), filtered (0.22 μm), and manually injected in an Agilent 1260 infinity system equipped with two Waters columns (Strygel HR2 and Strygel HR4E). The flow rate of 0.7 mL/min and volume of injection was 200 μL. Molecular weight was calculated based on polystyrene standards (3.7, 9.9, 13.0, 21.0, 44.0, and 76.0 kDa).

Preparation and Characterization of Empty and Drug-Loaded Polymeric Micelles. Polymeric micelles (PCL- or PBCL-based ones) containing conjugated Cy5.5 were prepared by mixing the synthesized block copolymers in the proportion described in Table S1. The concentration of Cy5.5 dye in the mixed micelles was 0.4 μg/mg of polymer, whereas the GE11 density was 5−20% mol/mol of the polymer (depending on the peptide feed ratio).

The A83B4C63 was physically encapsulated into the polymeric micelles by dissolving it (3 mg) together with the block copolymers (10 mg) in acetone. The ratio of unmodified and GE11 modified block copolymers used in the micellar composition was the same as that reported in Table S1. Then, the polymer/drug solution in acetone was transferred dropwise to double distilled water (10 mL) under constant stirring and kept overnight. The obtained micellar solutions were centrifuged at 11 600g for 5 min and then filtered through 0.22 μm membrane to remove free unencapsulated compound and/or possible polymeric aggregates.

The ζ-potential (ZP) of the prepared polymeric micelles was measured with a Zetasizer Nano (ZEN3600, Malvern Instruments, Worcestershire, U.K.). This equipment was also used for dynamic light scattering (DLS) experiments, in which micellar average diameter and its distribution, micellar thermodynamic stability, and micellar kinetic stability in the presence of sodium dodecyl sulfate (SDS) were determined, as reported before.[37,38] For critical micellar concentration (CMC) measurements, empty polymeric micelles were prepared in different concentrations (ranging from 0.49 to 500 μg/mL), and the count rate of scattered light was recorded. For the determination of micellar kinetic stability, polymeric micelles without drug were prepared to have a concentration of 2 mg/mL and incubated with the micellar destabilizing agent SDS at a concentration of 6.7 mg/mL. All DLS analyses were carried out at 25.0 ± 0.1 °C with a 173° scattering angle on identical polymer mixtures as detailed in Figure 1 and Table S1 without Cy5.5 to avoid interference in the DLS readings.

The morphology of all polymeric micelles was assessed by transmission electron microscopy (TEM). An aliquot of 10 μL of each micellar solution (polymer concentration of 0.5 mg/mL) was transferred to a copper-coated grid and incubated at room temperature for 15 s. After that, the samples were dried using Whatman filter paper and stained with 2% phosphotungstic acid solution, which was also removed using filter paper after 2 min of staining. Then, samples were analyzed in a Morgagni 268 TEM microscope (Philips/field emission) and image acquisition was performed using a Gatan CCD camera.

***In Vitro* Release of the Encapsulated A83B4C63.** The *in vitro* release of A83B4C63 from the polymeric micelles was assessed using the equilibrium dialysis method. Sets of dialysis tubing were prepared in triplicate, containing 2 mL of each micellar formulation. The release study was carried out at 37 °C for 48 h in 300 mL of distilled water, changing media periodically to ensure sink conditions and under shaking at 65 rpm in a water bath system (Julabo SW 22, Seelbach, Germany). At selected time points (0, 1, 2, 4, 6, 8, 24, and 48 h), aliquots of 200 μL were collected from inside the dialysis bags. The drug was quantified using reversed-phase chromatography (Varian Prostar 210 HPLC system, Palo Alto, CA, USA) coupled with a Microsorb-MV (Agilent Technologies (Little Falls, CA, USA) 5 μm C18 100 Å column (4.6 mm × 250 mm). The sample injection was 20 μL, the mobile phase was 0.1% trifluoroacetic acid and acetonitrile, and the flow rate was 0.7 mL/min at room temperature. Detection was performed at 280 nm, using a Varian 335 photodiode array HPLC detector (Varian Inc.).

Molecular Modeling of Binding between EGFR and Its Ligands GE11 and EGF. The structure of the extracellular domain of human epidermal growth factor receptor (EGFR) in complex with its physiological ligand (epidermal growth factor, EGF) was obtained from the Protein Data Bank (PDB code 1NQL) with a resolution of 2.8 Å.[39] The structure was refined and repaired by adding missing side-chains and assigning partial charges using Chimera.[40] Autoligand module of Autodock was used to identify the possible binding site for GE11 by scanning the highest affinity binding pockets on the surface of the protein.[41] The 3D structure of GE11 was built and prepared using the DOCKPREP module of Chimera, in the framework of the AMBER99SB force field. The docking protocol was performed using Autodock Vina by "boxing" the identified binding pocket into a grid of 100 Å × 100 Å × 100 Å, with a spacing of 0.375 Å.[42] To increase the accuracy of the docking, a total of 24 runs were performed with exhaustiveness of 40.

Before performing the molecular dynamic (MD) simulations, the structure of GE11 was parametrized using AnteChamber PYthon Parser interfacE (ACPYPE).[43] In order to predict the stability of GE11 in the predicted binding site and to calculate the binding free energy of the binding interactions, we used the GROMACS 5.1.5 package to perform a series of 20 ns long MD simulations for the structures of (a) apo GE11, (b) EGFR/GE11, and (c) EGFR/EGF complex.[44] The MD simulation of GE11 was carried out to obtain the most stable conformation of the molecule for both docking and the subsequent MD simulation. The simulation system was solvated in a box having 1 nm distance from each side, with TIP3P-modeled water molecules. Then, the system was neutralized using NaCl to reach a theoretical concentration of 0.15 M. The energy of the system was initially minimized using the AMBER99SB-ILDN force field, followed by heating to 300 K and equilibration (for 500 ps) using the Berendsen thermostat. After that, a series of 20 ns long production runs were performed for both complexes using periodic boundary conditions. Particle mesh Ewald (PME) algorithm was used to

https://doi.org/10.1021/acs.molpharmaceut.1c00918
Mol. Pharmaceutics 2022, 19, 1825−1838

calculate long-range interactions. All visualizations were carried out using the Schrodinger's PyMOL package (Molecular Graphics System, version ~1.8, 2015). Finally, the molecular mechanics Poisson−Boltzmann surface area (MMPBSA) module of Gromacs was used to compute the free energy of GE11 binding interactions in the last 5 ns of each simulation.[45] All the graphs were plotted using Grace and Prism version 7.00 (GraphPad Software, La Jolla, CA, USA).

Cell Lines. Colorectal cancer cell lines HCT116 and SW620 (wild type) were purchased from the American Type Culture Collection (ATCC). The cells were grown in Dulbecco's modified Eagle medium supplemented with 10% FBS, 1% penicillin−streptomycin solution at 37 °C in a 5% CO_2 atmosphere. Two approaches were used for genetically modifying the HCT116 cell line. For luciferase expression, cells were transfected with pEGFPLuc2 vector using Lipofectamine 2000 reagent,[46] while PTEN-deficient HCT116 cells, generated using Cre-LoxP technology,[47] were kindly provided by Dr. Todd Waldman (Georgetown University). EGFR expression was assessed for all cells used (i.e., wild-type and genetically modified ones) by Western blot.

***In Vitro* Cellular Uptake Studies.** HCT116 and SW620 cells were seeded into 12-well plates until reaching 70% confluence. GE11-modified and plain mixed micelles containing Cy5.5 covalently attached to the core-forming segment were added at a concentration equivalent to 0.2 μg/mL of Cy5.5 in each well in triplicate and incubated for 3 h at 37 °C. After the incubation time, cells were washed three times with cold PBS and trypsinized. A solution of 4% paraformaldehyde in PBS was added to fix the cells, and 10 000 events of single cells were recorded using the LSR-Fortessa X20 SORP (BD Biosciences, Franklin Lakes, NJ, USA). The cell-associated Cy5.5 was excited using a red-diode laser (635 nm), and the FL4 channel (675 nm) was used to detect the cell-associated median fluorescence intensity.

For confocal microscopy studies, the above CRC cells were seeded into 24-well plates containing round coverslips (0.2 mm thickness) at densities of (4−5) × 10^4 cells/well and incubated at 37 °C for 24 h until they were 50% confluent. Cy5.5-labeled plain or GE11-modified PEO-PBCL micelles (0.2 μg/mL Cy5.5) were added to the wells in triplicate and incubated for 3 h at 37 °C. After that, cells were washed three times with cold PBS and fixed for 10 min using 4% paraformaldehyde. Then, the coverslips were removed and inverted on a slide with a drop of mounting media containing DAPI. The slides were allowed to cure in the dark for 24 h. The analysis of cell associated Cy5.5 was carried out by an inverted confocal microscope, Quorum WaveFX spinning disk confocal system (Quorum Technologies Inc., Guelph, Canada). Images were acquired with an oil immersion lens with 40× objective. Fluorophores were excited at 405 nm (for DAPI) and 633 nm (for Cy5′s). The emitted fluorescence was detected through spectral channels at 410−500 nm and 633−744 nm for blue and red fluorescence, respectively. The images were acquired and analyzed using Volocity software (PerkinElmer, Waltham, MA, USA).

Western Blot. Expression of EGFR by SW620 and HCT116 cell lines as well as HCT116-*luc2*$^+$*PTEN*$^{+/+}$ and HCT116-*luc2*$^+$*PTEN*$^{-/-}$ was evaluated at the protein level. Cells were seeded in six-well plates, and once 70% confluence was reached, they were washed with PBS and lysed (in RIPA buffer). The lysis buffer was supplemented with PMSF, protease, and phosphatase inhibitor, and the cell lysates were incubated for 30 min on ice, followed by centrifugation at 21 000*g* for 20 min. After protein quantification, using a BCA protein assay kit, an equal amount of protein was resolved through gel electrophoresis and transferred to a nitrocellulose membrane. Membranes were probed with rabbit antibodies against EGFR and β-actin. Finally, protein revelation was done using peroxidase-conjugated anti-rabbit IgG and detected by chemiluminescence. The relative protein expression was estimated through band densitometry using ImageJ software (version 1.53a, National Institutes of Health, USA).

Cell Proliferation Assays. *In vitro* viability of CRC cells following treatment with A83B4C63 and its encapsulated form in plain and GE11 micelles was evaluated by measuring cellular metabolic activity and luminescence signal of HCT116-*luc2*$^+$*PTEN*$^{-/-}$ cells. Cells were seeded in a 96-well plate, and once 70% confluence was reached, cells were treated with increasing concentrations of A83B4C63 as part of different formulations. For 3-(4,5-dimethylthiazol-2-yl)-2,5-diphenyltetrazolium bromide (MTT) assays, 20 μL of MTT solution (5 mg/mL) was added to treated cells and incubated at 37 °C for 2 h. The medium was then replaced by 100 μL of DMSO, and the absorbance was read at 570 nm (Synergy H1 hybrid reader, Biotek). For the second measurement, cells were treated for 5 min with D-luciferin (20 mg/mL), and the luciferase activity was recorded by luminescence using the IVIS imaging system (Caliper Life Sciences; Alameda, CA, USA).

Animal Models. Athymic (*nude/beige*) NIH-III mice were purchased from Charles River (Wilmington, MA). All animal studies were conducted in accordance with the guidelines of the Canadian Council on Animal Care (CCAC) with approval from the Animal Care and Use Committee (ACUC) of the University of Alberta (Edmonton, AB, Canada) and University of Calgary (Calgary, AB, Canada). Mice were fed using the 2014S Teklad Global 14% protein rodent maintenance diet to minimize fluorescence interference from chlorophyll. The orthotopic CRC mouse model was developed similarly to the one described previously with some modifications.[48] In summary, the intestine of each mouse was exposed by surgery, and 50 μL of solution containing 0.5 × 10^6 HCT116-*luc2*+ cells and 50% Matrigel basement membrane matrix (BD Biosciences, Franklin Lakes, NJ, USA) was injected in the cecum wall. When the tumors became detectable by luminescence measurement, the treatments were initiated. Animals were monitored daily for any sign of abnormal behavior or weight loss.

***In Vivo* Imaging and Tissue Biodistribution Study.** Animals (NIH-III nude mice) were injected through tail vein iv administration, with the following Cy5.5-tagged mix micelles: PEO-PCL, GE11-PCL, PEO-PBCL, and GE11-PBCL (Table S1). The micellar concentration was 250 mg/kg of body weight (equivalent to 0.1 mg/kg of free Cy5.5), as described in our previous report.[36] At different time-points after injection (2, 6, and 24 h), fluorescence and luminescence signals in live mice were measured using the Xenogen IVIS imaging system instrument (Caliper Life Sciences; Alameda, CA, USA). For bioluminescence imaging, D-luciferin (150 mg/kg) was subcutaneously injected into the mice 5 min prior to the measurements. Animal images and readings were analyzed with Living Image 3.0 software (Caliper Life Sciences). Lastly, at 24 h postinjection, mice were euthanized for *ex vivo* studies. Tumors and other organs (liver, kidneys, lung, intestine, spleen, heart, and brain) were excised, incubated in D-luciferin

https://doi.org/10.1021/acs.molpharmaceut.1c00918
Mol. Pharmaceutics 2022, 19, 1825−1838

Table 1. Characteristics of Block Copolymers in the Preparation of Mixed Micelles[a]

block copolymers	Mn (g/mol)	degree of polymerization (DP) per segment			Cy5.5 conj (molar % ± SD)	GE11 conj (molar % ± SD)
		PEO	P(B)CL	PPC		
PEO-*b*-PCL	7800	114	24.5			
GE11-PEO-*b*-PCL	9300	123	24.3			78.7% ± 2.5
PEO-*b*-PCL-*b*-P(CL-*g*-Cy5.5)	9700	114	23.7	2.9	2.4 ± 0.3	
PEO-*b*-PBCL	10900	114	23.6			
GE11-PEO-*b*-PBCL	12600	123	24.4			70.2% ± 2.2
PEO-*b*-PBCL-*b*-P(CL-*g*-Cy5.5)	13200	114	25.3	2.7	5.9 ± 1.1	

[a]The composition of mixed micelles in different groups are listed in Table S1.

Table 2. Physicochemical Characteristics of Polymeric Micelles under Study[a]

mixed micelles	size (nm)	PDI	ZP (mV)	CMC (nM)	EE (%)
PEO-PCL	56.5 ± 0.5[a]	0.24	−0.75 ± 0.21[a]	368 ± 0.02[a]	
GE11-PCL	53.5 ± 0.1[b]	0.23	−3.48 ± 0.55[a,b]	419 ± 0.05[b]	
PEO-PCL + A83	54.3 ± 0.1[c]	0.20	−9.91 ± 0.64[c]		74.0 ± 2.8[a,b]
GE11-PCL + A83	55.3 ± 0.1[d]	0.22	−16.8 ± 1.48[d]		72.1 ± 3.5[a]
PEO−PBCL	39.9 ± 0.3[e]	0.21	0.99 ± 0.36[a]	95 ± 0.02[c]	
GE11-PBCL	41.5 ± 0.2[f]	0.26	−5.16 ± 0.78[b]	167 ± 0.01[b]	
PEO-PBCL + A83	40.1 ± 0.2[e]	0.18	−6.92 ± 1.98[b,c]		79.5 ± 1.4[b,c]
GE11-PBCL + A83	42.2 ± 0.3[f]	0.16	−16.0 ± 2.55[d]		80.8 ± 2.1[c]

[a]Letters superscripted in each column indicate the results after statistical analysis (one-way ANOVA, Tukey's *post hoc* test). Values (n = 3) bearing the same letters are not significantly different from each other ($p > 0.05$), and in the opposite case, their differences are significant ($p < 0.05$).

solution (300 μg/mL), and imaged for fluorescence and bioluminescence using the IVIS instrument.

***In Vivo* Therapeutic Activity of A83B4C63 Loaded into Micelles.** Mice were treated (tail vein iv administration) with six doses of A83B4C63, with each dose (25 mg/kg physically loaded into PEO-PBCL and GE11-PBCL micelles) administered every other day (n = 3). Tumor growth was monitored every 3−5 days through luminescence measurement, after 7 min of D-luciferin (150 mg/kg) subcutaneous injection using the Xenogen IVIS imaging system instrument. A threshold of 2×10^7 p s^{-1} cm^{-2} sr^{-1} for luminescence by primary tumors was established as the end point for the study. Images and intensities were processed using the Living Image 3.0 software (Caliper Life Sciences).

Statistical Analysis. Data are presented as the mean ± standard error of the mean (SEM). When suitable, the data were analyzed for statistical significance using unpaired Student's t test or one-way analysis of variance (ANOVA) followed by Tukey's *post hoc* test. The minimum level of significance was set for $p < 0.05$.

RESULTS

Characterization of Synthesized Block Copolymers and Associated Micelles. The characteristics of the block copolymers under study are summarized in Table 1. The PEO-PCL and PEO-PBCL block copolymers had a number-average molecular weight (M_n) of 7800 and 10 900 g/mol, respectively, based on ^{1}H NMR analysis (Figures S1 and S2), while a M_n of 7200 and 9600 g/mol, respectively, was determined by SEC experiments (Table S2). Both techniques indicated that the values of M_n correspond approximately to the calculated degree of polymerization (DP) of 25, initially designed for PCL and PBCL segments. The chromatographic analysis revealed that the dispersity is somewhat higher in PEO-PBCL (Đ = 2.78) than in PEO-PCL (Đ = 1.46) copolymers. Moreover, the 2D DOSY NMR results (Figure S3) further corroborated that the diblock copolymers were successfully synthesized and purified, since no traces of free monomer or PEO homopolymer were identified. The molar conjugation of peptide to polymer in GE11-PEO-PCL and GE11-PEO-PBCL was 79% and 70%. For PEO-PCL-P(CL-*g*-Cy5.5) and PEO-PBCL-P(CL-*g*-Cy5.5), fluorescent spectroscopy confirmed the attachment of Cy5.5 into the PPC segments, and the quantification results showed the Cy5.5 molar conjugation percentage to the polymer was 2.4% and 5.9%, respectively. The DP of PCL and PBCL remained around 24−25 in GE11- or Cy5.5-modified block copolymers as determined by ^{1}H NMR (Table 1).

For NIR imaging studies, as depicted in Figure 1, the Cy5.5-labeled polymeric micelles, abbreviated as GE11-PCL micelles, were prepared by mixing PEO-*b*-PCL (6.8 mg), GE11-PEO-*b*-PCL (1.2 mg), and PEO-*b*-PCL-*b*-P(CL-*g*-Cy5.5) (2.0 mg), while GE11-PBCL micelle preparation was performed by combination of PEO-*b*-PBCL (8.0 mg), GE11-PEO-*b*-PBCL (1.4 mg), and PEO-*b*-PBCL-*b*-P(CL-*g*-Cy5.5) (0.6 mg). This corresponds to a density of 10% (mol/mol) for GE11 on the micellar structure. To change the density of GE11 for cell uptake studies (i.e., 5% and 20% mol/mol), the proportion of copolymers was adjusted accordingly. Control micelles, having no peptide decoration, were made up using the same approach but without mixing the GE11-containing block copolymers. The composition of each Cy5.5-tagged polymeric micellar system is listed in Table S1.

For the assessment of anticancer activity, GE11-modified mixed micelles were prepared through a combination of PEO-*b*-PCL or PEO-*b*-PBCL and their corresponding GE11-modified copolymer counterparts, together with A83B4C63, which were dissolved in acetone prior to the micellization. Plain micelles carrying A83B4C63 were prepared using PEO-*b*-PCL or PEO-*b*-PBCL alone. A cosolvent evaporation method was used for the micellization process, and Table S1

https://doi.org/10.1021/acs.molpharmaceut.1c00918
Mol. Pharmaceutics 2022, 19, 1825−1838

comprehensively shows how the block copolymers were combined for the preparation of each micellar formulation.

The characteristics of prepared micellar formulations are summarized in Table 2. All polymeric micelles used in this study showed a low polydispersity index (PDI < 0.3). The PBCL-based micelles (~41 nm) were smaller in diameter than the PCL-based ones (~55 nm) ($p < 0.05$; unpaired t test). The incorporation of A83B4C63 into the micellar structure did not affect particle size in PBCL-based micelles ($p > 0.05$; one-way ANOVA, Tukey's *post hoc* test), but micellar size was significantly affected by A83B4C63 incorporation in PCL-based ones ($p < 0.05$; one-way ANOVA, Tukey's *post hoc* test). The direction of diameter changes following drug incorporation did not follow a specific trend for PCL based micelles though. The average diameter of plain micelles versus GE11 micelles showed that the peptide incorporation contributed to increasing of the micellar particle size for both empty and loaded micelles. Regarding the morphology of A83B4C63 micellar formulations, the TEM images (Figure S4) indicated the formation of spheres and uniform size distribution pattern of the particles, though some shrinkage may have taken place due to their dry state, as reported for similar micellar structures.[49−51] Similar to our observations with the DLS (Table 2), the TEM data also showed larger micelles to be formed from PEO-PCL compared to PEO-PBCL ones.

Empty PEO-PCL and PEO-PBCL micelles showed a near neutral ζ potential. The ζ-potential of micelles became negative following GE11 surface modification for both PCL- and PBCL-based micelles ($p < 0.05$; one-way ANOVA, Tukey's *post hoc* test). This observation was in line with previous reports on other types of polymeric micelles,[29] further confirming the success of peptide conjugation. Drug encapsulation in plain and GE11-modified micelles led to an increase in micellar ZP as well.

Modification of micellar shells with GE11 did affect the CMC for both PCL and PBCL micelles (Table 2), leading to a significant decrease in micellar thermodynamic stability, reflected by an increase in CMC ($p < 0.05$; one-way ANOVA, Tukey's *post hoc* test). Moreover, micelles with PBCL structure in their core showed a much lower CMC compared to the ones with PCL cores irrespective of peptide modification ($p < 0.05$; one-way ANOVA, Tukey's *post hoc* test).

Unlike PBCL-based micelles, which were shown to be kinetically stable, a substantial decrease in the intensity of PCL-based micelles was observed following incubation with SDS (Figure 2A,B). Incubation of plain- or GE11-modified PBCL based micelles with SDS did not affect the kinetic stability of these structures.

PEO-PCL and GE11-PCL micelles showed an average encapsulation efficiency of 74.0% and 72.1% for A83B4C63, respectively. This value for PEO-PBCL and GE11-PBCL micelles was 79.5% and 80.8%, respectively (Table 2). In general, PBCL-based micelles showed higher encapsulation of A83B4C63, without or with peptide on their surfaces ($p < 0.05$; unpaired t test). In both micellar core structures, no difference in the encapsulation of A83B4C63 between plain and GE11-modified ones was observed ($p > 0.05$, one-way ANOVA). Furthermore, >70% of the drug was released from the micelles with PCL cores within 8 h (72.6% for PEO-PCL micelles and 88.8% for GE11-PCL micelles), as shown in Figure 2C, whereas PBCL micelles showed <50% drug release at that same time point (42.7% for PEO-PBCL micelles and

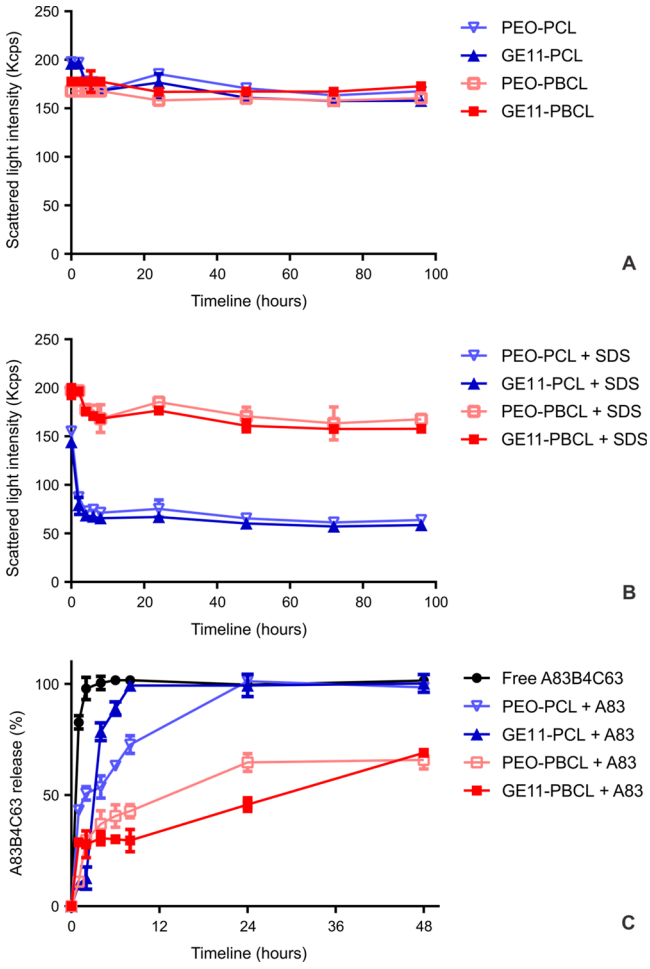

Figure 2. Micellar kinetic stability profile: (A) in water; (B) in the presence of sodium dodecyl sulfate (SDS, 6 mg/mL); (C) *in vitro* release of A83B4C63 as free drug or loaded in plain and GE11 micellar formulations.

29.5% for GE11-PCL micelles, on average). While drug release for PCL micelles was nearly 100% at 48 h, only 65.7% and 68.9% of the A83B4C63 were released from PEO-PBCL and GE11-PBCL micelles, respectively, at that same time point.

Binding Mode and Binding Free Energy of GE11 versus EGF to EGFR. The predicted human EGFR binding site for the GE11 peptide was found to be different from that of EGF (Figure 3). The free energy for binding interactions calculated for GE11-EGFR and EGF-EGFR complexes were −163.43 kJ/mol (−39.06 kcal/mol) and −621.68 (−148.58 kcal/mol), respectively (Table 3). This difference in binding free energies for these two ligands indicates that EGF binding is 3.8-fold more spontaneous and is consistent with previous observations reported in the literature.[23] Figure S5 shows the interacting side-chain amino acid residues involved in both complexes during the MD simulations. The root-mean-square fluctuation (RMSF) analysis of the EGF and GE11-EGFR complexes side chains corroborated the initial docking poses, showing that both entities under investigation maintain contact with the residues illustrated in Figure 3 during the length of the MD simulation (Figure S5A−C). The backbone RMSD of GE11/EGFR and EGF/EGFR complex shows reasonable stability for the EGFR backbone during the MD simulation of both complexes. However, ligand positional RMSD calcu-

https://doi.org/10.1021/acs.molpharmaceut.1c00918
Mol. Pharmaceutics 2022, 19, 1825−1838

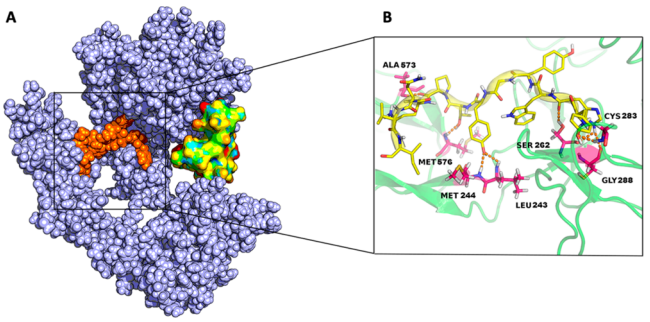

Figure 3. Molecular dynamics (MD) simulations using the crystal structure of human EGFR: (A) prediction of the binding site of EGF (in rainbow) and GE11 (in orange) with EGFR; (B) identification of the main intermolecular interactions between GE11 and EGFR. Polar contacts are shown by broken orange lines.

lations showed that the EGF-EGFR is more stable than the GE11-EGFR complex (Figure S5B).

GE11-Containing Micelles Are Highly Internalized by EGFR-Expressing Cells. Fluorescent signals from Cy5.5-labeled polymeric micelles, quantified by flow cytometry analysis, indicated that the overall micellar uptake by SW620 cells was lower compared to HCT116 cells (Figures 4 and S6). Despite this difference in endocytosis rate, PCL- and PBCL-based micelles, with and without GE11 surface modification, exhibited similar uptake by SW620 cells. In contrast, GE11-modified micelles showed enhanced uptake by HCT116 cells compared to the plain micelles (Figure 4A). The observation was in line with the level of EGFR expression in these two cell lines as measured by Western blot (Figure S8).

The effect of peptide density on the micellar shell on the uptake of particles by SW620 and HCT116 cells was also tested for PBCL-based micelles. The results showed a similar level of micellar uptake, irrespective of GE11 density, by SW620 cells. In contrast, increasing the levels of GE11 peptide on the micellar surface contributed to an increase in cell-associated fluorescence in EGFR-positive HCT116 cells. The exception was a nonsignificant difference between the uptake of micelles with 10 and 20 mol % of GE11, suggesting saturation of cell surface EGFR at the 10% level. Confocal microscopy (Figure S7) confirmed the preferential internalization of GE11 micelles in HCT116 cells as compared to that of plain micelles or uptake in SW620 (EGFR negative) cells.

***In Vivo* Distribution of GE11-Modified versus Plain Polymeric Micelles in Orthotopic HCT116 Luc+ Xenograft Model.** The tumor location was identified by luminescence imaging and used to estimate micellar accumulation in the tumor for different groups under study. Metastasis was observed in all organs in most of the cases except for the brain.

Images of plain or GE11-modified micellar biodistribution following intravenous injection in orthotopic HCT116 Luc+ xenografted NIH III mice are shown in Figure 5. More rapid clearance of PCL-based micelles within 24 h possibly through the kidneys was observed. On the other hand, PBCL-based micelles appeared to stay longer, showed higher levels in normal organs, and were perhaps mainly cleared by the liver since this organ presented the strongest fluorescence.

In live animals, higher tumor accumulation of Cy5.5-labeled PCL-based micelles (either plain or GE11-modified) was achieved at the 2 h time point compared to the PBCL-based micelles ($p < 0.05$, unpaired t test). However, over time this pattern shifted so that at 6 h postinjection, the micellar fluorescence signals were comparable among all micelles under study. By 24 h, the tumor accumulation of PEO-PBCL micelles was higher than that of PEO-PCL micelles ($p < 0.05$; unpaired t test).

When comparing the PEO-PCL micelles with their GE11-modified counterparts, no difference in tissue distribution was noticeable in live mice (Figure 5A). For PEO-PBCL micelles versus GE11-PEO-PBCL however, a confinement of the distribution to tumor and surrounding areas in live mice was noticeable for the GE11-modified structures but not for unmodified PEO-PBCL.

The above analysis in live animals provided an estimate for the distribution of different micellar formulations in orthotropic tumors. However, depending on the distribution of particles among organs that reside near the region where the cecum is located, such as spleen and liver, an overestimation of micelle accumulation in the orthotopic tumor model may have occurred. The analysis of the excised organs contributed to a clearer insight about micellar biodistribution. This analysis was conducted at 24 h postinjection (Figure 6).

Among different excised organs, kidneys were the only organ that showed a comparable distribution among PCL and PBCL micelles; all other examined organs, i.e., liver, lungs, and heart, illustrated a considerably stronger fluorescent signal for PBCL-based micelles. A trend toward higher accumulation of PBCL-based micelles compared to PCL-based ones was also observed in the spleen, though there was no statistical significance. The GE11 modification of polymeric micelles did not seem to lead to enhancement in tumor accumulation of the carrier at 24 h postinjection, irrespective of the micellar core structure (Figure 6B). Analysis of the excised intestines (whole intestine) from animals with tumor growth pointed to a trend in increased accumulation of GE11-modified micelles compared to their plain (unmodified) counterparts, but the difference was not statistically significant (data now shown). At the same time point, accumulation in other normal organs was also not affected by the GE11 modification of polymeric micelles irrespective of the presence or absence of metastatic cells. The results also suggest that none of the prepared polymeric micellar systems were able to cross the blood−brain barrier since no signal was detected in the brain.

Table 3. Calculated Free Energy of Binding to EGFR for EGF and GE11 (MMPBSA)[a]

EGFR ligand	van der Waals energy (kJ/mol)	electrostatic energy (kJ/mol)	polar solvation energy (kJ/mol)	SASA energy (kJ/mol)	binding energy (kJ/mol)
EGF	−558.426 ± 33.4	−395.031 ± 116.3	392.68 ± 60.5	−60.908 ± 3.6	−621.68 ± 165.72
GE11	−234.07 ± 27.3	−192.73 ± 42.9	292.64 ± 66.2	−29.264 ± 3.5	−163.43 ± 33.08

[a]The free energy of binding was calculated by summing the van der Waals, solvent-accessible surface area (SASA), and electrostatic energy and subtracting the polar solvation energy.

https://doi.org/10.1021/acs.molpharmaceut.1c00918
Mol. Pharmaceutics 2022, 19, 1825−1838

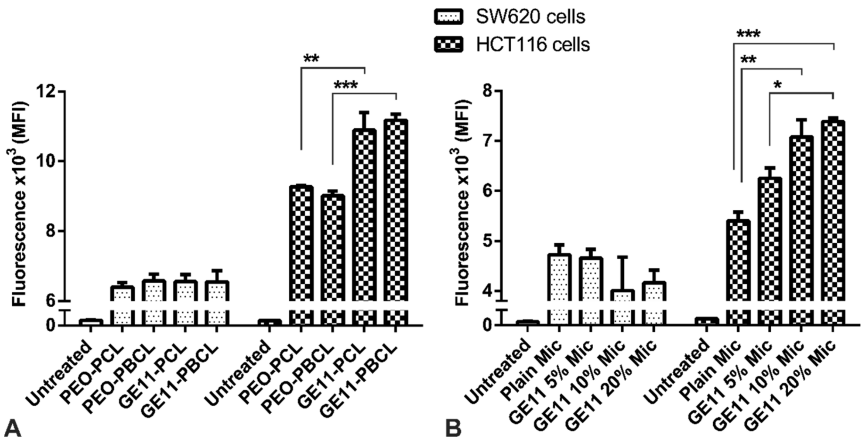

Figure 4. *In vitro* uptake of Cy5.5-labeled mix micelles by colorectal cancer cell lines. Flow cytometry data show median fluorescence intensity (MFI) measured after 3 h treatment at 37 °C. (A) Effect of GE11 modification on PCL- and PBCL-based micelles in peptide density of 10% (mol/mol). (B) Effect of PBCL-based micelles with different surface peptide densities. $*p < 0.05$, $**p < 0.01$, $***p < 0.001$. Data are presented as mean ± SEM.

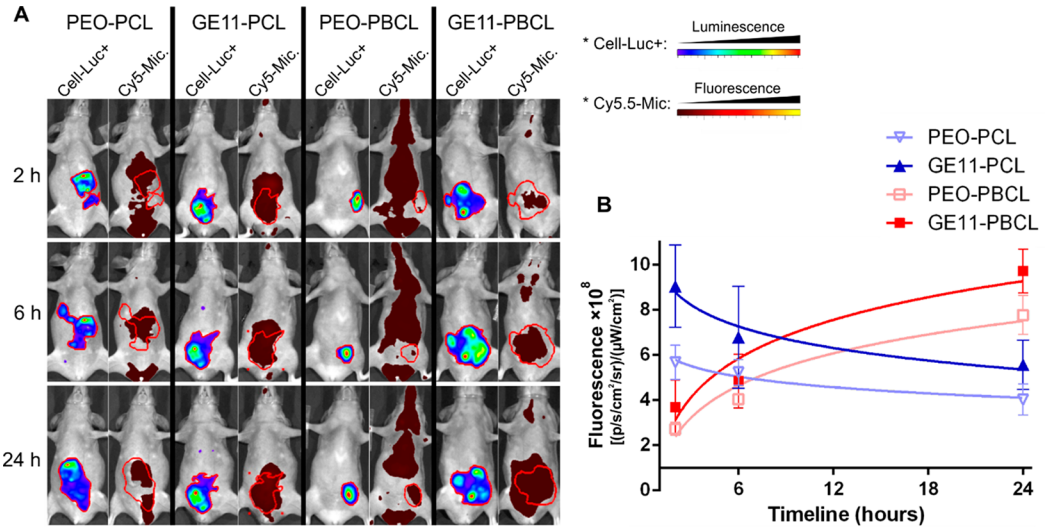

Figure 5. *In vivo* imaging of Cy5.5-tagged mixed micelles after 2, 6, and 24 h intravenous administration. (A) Each time-point contains one representative capture of luminescence (tumor signal[1]) and fluorescence (micelles[2]). (B) Graph shows fluorescence intensity coming from the Cy5.5-labeled polymeric micelles at the region colocalizing with luminescence signals.

Therapeutic Activity of A83B4C63 Nanoformulations. We conducted studies evaluating the anticancer activity of encapsulated A83B4C63 in plain versus GE11-modified micelles, against HCT116-*luc2*$^{+}$*PTEN*$^{-/-}$ tumors *in vitro* and *in vivo*. All empty micelles were found to be nontoxic against the referred CRC cells at a polymer concentration equivalent to the 50 μM drug (Figure S9). As shown in Figure 7, encapsulated A83B4C63 in PCL-based micelles appeared to be more effective in reducing cell proliferation compared to PBCL-based formulations of this drug. This observation was in line with a slower release of A83B4C63 from the PBCL based micelles. GE11 modification of the micellar surface contributed to enhancing of the therapeutic activity of PBCL-based micellar formulations of A83B4C63 at drug concentrations of ≥12.5 μM (Figure 7D). The effect of GE11 modification of the micellar formulation was not observed for GE11-PCL micelles at least up to 50 μM A83B4C63.

PBCL-based micelles were able to provide a controlled release profile of the A83B4C63 compound within 48 h (e.g., the release from GE11-PBCL was 2.2-fold slower than GE11-PCL), as well as a higher tumor accumulation *in vivo* over the PCL-based ones at 24 h. Thus, the evaluation of the drug activity was performed using only nanoformulations composed of PEO-PBCL and GE11-PBCL micelles. The results of this study are summarized in Figure 8. The *in vivo* image of tumor growth in the longest surviving mice in each group is shown in Figure 8A. As shown here, the longest survival for mice receiving 5% dextrose vehicle was 37 days, whereas this duration was extended to 54 and 72 days for the longest surviving mice treated with plain and GE11-modified PBCL based micelles of A83B4C63, respectively. Figure 8B shows the rate of tumor growth in the animal of different groups. Mice receiving dextrose were the first group in which the luminescence signal, from the orthotopically implanted CRC cells, reached the threshold level. This was followed by the group treated with the plain PEO-PBCL formulation of A83B4C63 and, later, by the group that received the A83B4C63 loaded into GE11-PBCL micelles. The effect of GE11 modification on this formulation significantly contributed to lowering of tumor growth when compared with the

https://doi.org/10.1021/acs.molpharmaceut.1c00918
Mol. Pharmaceutics 2022, 19, 1825−1838

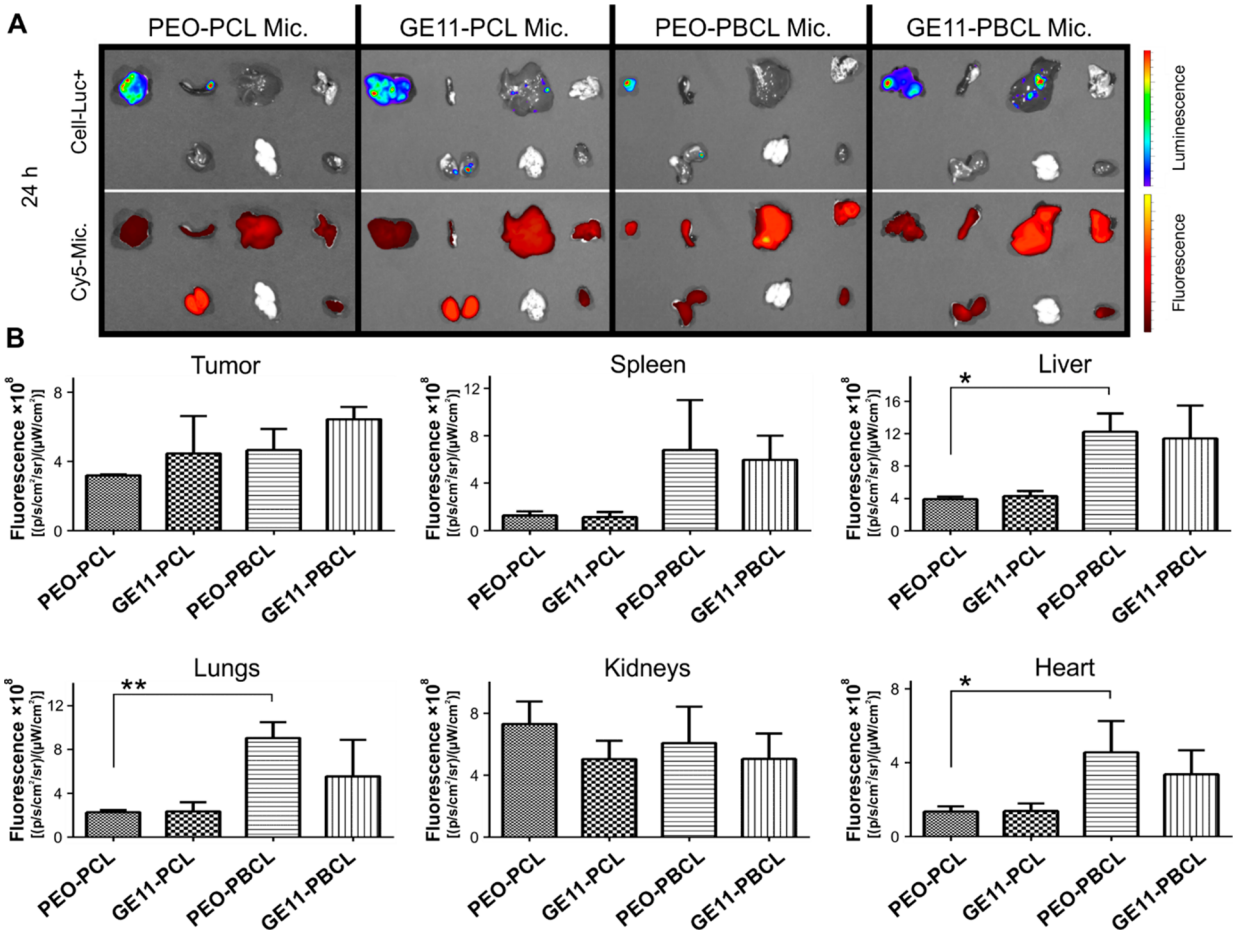

Figure 6. *Ex vivo* imaging of Cy5.5-tagged micelles 24 h after intravenous administration. (A) Images show (clockwise from top left corner) tumor, spleen, liver, lungs, heart, brain, and kidneys. Each excised organ is representative of one individual mouse from a group of three mice. For the tumor signal,[1] luminescence originated from the HCT116 luciferase positive cells. For the micelles signal,[2] fluorescence was from the Cy5.5 dye present inside the micelles. (B) The bar graphs represent the micelle accumulation in the organs after 24 h injection ± SEM: unpaired *t* test, $*p < 0.05$, $**p < 0.01$.

dextrose group at 37 days following initial treatment. Animals treated with dextrose and PEO-PBCL formulations presented a small impairment in weight gain (Figure 8C). The survival curves indicate that the A83B4C63 treatment using both formulations were effective in prolonging mouse lifetime when compared with the dextrose group, even though the treatment was slightly more beneficial when the GE11-modified formulation was applied (Figure 8D).

DISCUSSION

The interaction of Cy5.5-tagged polymeric micelles with and without GE11 ligand modification with $EGFR^+$ and $EGFR^-$ CRC cells showed an enhancement for the GE11-modified micelles at an effective GE11 density, i.e., >10% (mol/mol), with the HCT116 cells that express EGFR (Figure 4). This enhancement was observed for both PEO-PCL and PEO-PBCL micelles. In line with this observation, an increase in the activity of encapsulated A83B4C63 in $PTEN^{-/-}$ HCT116 cells by GE11-PEO-PBCL micelles (and not PEO-PCL ones) over plain micelles was seen (Figure 7). The observation was attributed to the ability of PEO-PBCL and its GE11-modified counterpart to prolong retention of their drug content, a property that could not be achieved by PEO-PCL based micelles (Figure 2).

The *in vivo* biodistribution and therapeutic activity of A83B4C63 loaded in GE11 and plain polymeric micelles were then evaluated in PTEN-deficient CRC using an orthotopic CRC model with local and distant metastasis. In line with other studies that also developed a similar form of orthotopic CRC model, we also found metastatic regions in the main organs among the inoculated mice, highlighting spleen, liver, and lungs (Figure 5).[48,52,53] The brain was the only organ that did not show any metastasis of CRC cells as evidenced by the lack of luminescence signal related to LUC+ HCT116 cells used in the current study. In the orthotopic CRC model, PEO-PBCL micelles showed longer residence and broader distribution in normal organs, particularly at early time points, when compared to PEO-PCL micelles. At later time points, i.e., 24 h following injection, the PEO-PBCL micelles appeared to be cleared gradually from normal organs and their distribution was more confined to the primary tumor location (Figure 5). This finding was in line with our previous observations in an orthotopic breast cancer model.[36]

When comparing the effect of GE11 modification, we observed an increasing trend that did not reach statistical significance for the accumulation of GE11-modified polymeric micelles compared to the plain ones in orthotopic HCT116 tumors 24 h postinjection, irrespective of the micellar core structure (Figure 8). This contrasted with our previous

https://doi.org/10.1021/acs.molpharmaceut.1c00918
Mol. Pharmaceutics 2022, 19, 1825−1838

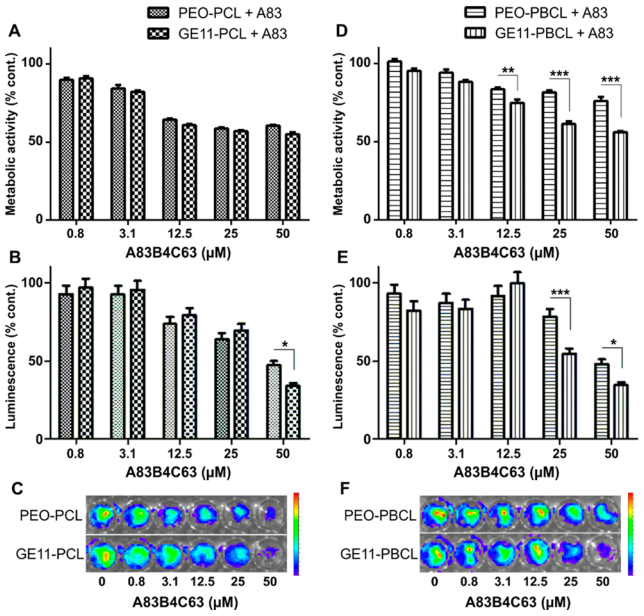

Figure 7. *In vitro* therapeutic activity of nanoformulated A83B4C63 in HCT116-*luc2*$^{+}$*PTEN*$^{-/-}$ cells. After 48 h treatment, the MTT assay was carried out using (A) PCL-based and (D) PBCL-based micelles. Luciferase activity was measured in parallel based on the luminescence signal. (B, E) Data presented by bar graphs, as well as by the images (C, F) of cell culture plates. The experiments were done in triplicate and are expressed as the mean ± SEM: unpaired *t* test, $*p < 0.05$, $**p < 0.01$, $***p < 0.001$.

observation in a subcutaneous HCT116 xenograft model using positron emission tomography (PET), where a significant increase in the accumulation of ^{64}Cu-labeled GE11-PEO-PBCL micelles compared to micelles with nontargeting peptide modification was seen.[18] The GE11 modification of PEO-PBCL micelles appears to reduce the distribution of these nanostructures in normal tissues and confines them to the tumor and surrounding tissues (Figures 5 and 8). This was not observed for the PEO-PCL micelles though.

To investigate any correlation between luminescence signal associated with the presence and number of tumor cells in different metastatic locations and micellar accumulation in that organ, we ran a correlation between normal tissue luminescence (except for brain) in all animals under study and micelle associated fluorescence signal from the same animal at 24 h postinjection. The results showed no correlation for any of the micellar structures under study (Figure S10). This may indicate that the micellar structures under study, even those with the GE11 modification, were not able to target tumor cells at metastatic sites at the present tumor cell load. Ligands with higher affinity for EGFR as well as greater biological stability than GE11 may be required for EGFR^{+} tumor cell targeting at metastatic sites.

Our MD simulation confirmed the relatively lower affinity of GE11 toward human EGFR when compared to its physiological ligand. This finding is in agreement with other reports that measured poorer dissociation constants for GE11 ($K_d \sim 4.59 \times 10^{-4}$ M) compared to EGF ($K_d \sim 1.77 \times 10^{-7}$ M).[23,54] In a previous MD simulation conducted by Ongarora et al.,[55] the GE11 binding site was shown to be relatively close to the location where EGF binds, though there was no further investigation in this regard. Our results corroborated those findings and additionally suggested that even though their binding sites are somewhat close to each other, they are actually in different locations. However, the binding energy of GE11 in that study was reported to be −24.93 kJ/mol, whereas in our *in silico* analysis, the binding energy was −163.43 kJ/mol.

Mickler et al.[27] demonstrated that the mechanism of EGFR cell internalization induced by GE11 is dependent on pre-existing connections between EGFR and the actin cytoskeleton. EGF might be able to trigger new connections to the cytoskeleton, making the receptor-mediated endocytosis possible even under the condition of cell starvation, which is known to lead to interruption in the connections between the EGFR and the actin cytoskeleton. Given the fact that cancer cells often suffer from restricted access to nutrients and oxygen in advanced stages of tumor progression,[56] the use of GE11-modified nanoparticles may be beneficial only against cancer cells located in the tumor periphery.

Considering the better *in vitro* and *in vivo* stability of PEO-PBCL micellar formulation of A83B4C63 and its GE11-modified counterpart (Figures 2 and 4−7), these formulations were further tested for their *in vivo* anticancer activity as nanotherapeutics in an orthotopic CRC model. Our previous studies have shown the activity of PEO-PBCL micellar formulations of A83B4C63 in PTEN^{-} HCT116 subcutaneous tumors as monotherapy by the process of synthetic lethality. The data in the current study revealed a trend toward better activity for the GE11-modified PEO-PBCL micellar formulation of A83B4C63 in reducing the growth rate of orthotopic primary and metastatic PTEN^{-} HCT116 tumors in comparison to the plain micellar formulations of this compound. Although the data provided proof of principle evidence for the potential benefit of EGFR targeted polymeric micellar formulations of A83B4C63 as single therapeutics for aggressive and metastatic tumors, the benefit of GE11-modified micellar formulations over plain micelles did not reach statistical significance (Figures 5 and 6B). This could be attributed to lower affinity of GE11 toward human EGFR, as demonstrated by our MD simulation analysis (Table 3) and/or low stability of this peptide in micellar conjugated form within biological media.

After the discovery and characterization of GE11, little has been done regarding peptide optimization, especially toward lowering proteolytic degradation in the presence of human serum.[23,57] More recently, this peptide sequence was reported to present poor stability against proteolysis ($t_{1/2} \sim 1$ h), which confirms the need for more investigation into improving its stability against chemical degradation.[25] Peptide cyclization is an interesting approach that has already been implemented with successful outcomes. This issue represents a special concern when the peptide is attached to the surface of nanoparticles, given their longer *in vivo* circulation.[58,59]

CONCLUSIONS

The GE11 micellar shell modification showed a clear benefit in enhancing the interaction and activity of encapsulated A83B4C63 in EGFR^{+} CRC cells, *in vitro*. The GE11-modified micelles showed a trend in enhancing the accumulation of micellar carrier in primary orthotopic HCT116 tumors and a significant reduction of tumor growth when loaded with A83B4C63, *in vivo* compared to untreated controls. The data provided incentive for the development of micellar structures with EGFR ligands of higher affinity and biological stability than GE11 and may lead to better tumor targeting and activity

https://doi.org/10.1021/acs.molpharmaceut.1c00918
Mol. Pharmaceutics 2022, 19, 1825−1838

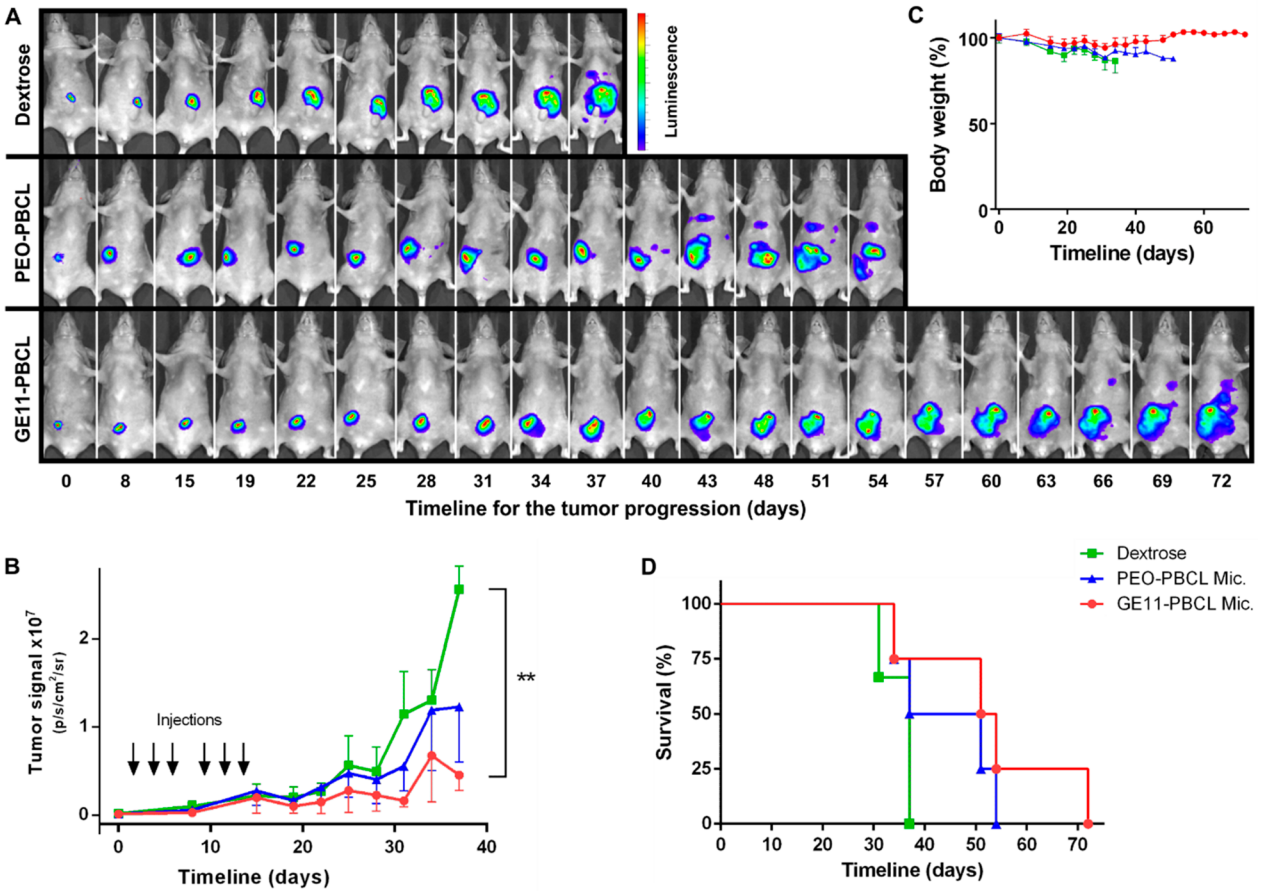

Figure 8. *In vivo* treatment with A83B4C63 loaded into PBCL-based micelles. NIH-III nude mice, implanted with HCT116-Luc2+ *PTEN*−/− cells orthotopically, received 6 iv injections of 25 mg/kg of the PNKP inhibitor. (A) Luminescence images of the individual mouse with highest survival from each group. (B) Tumor growth rate measured by luminescence signal. (C) Mean percentage change in animal body weight. (D) Survival curves for the three groups tested. Values are the mean ± SEM (n = 3): unpaired t test, $^{**}p < 0.01$.

against EGFR$^+$ tumors. Future studies will focus on the development and evaluation of such ligands in targeted delivery of therapeutics to mCRC on their own or on the surface of nanocarriers.

■ ASSOCIATED CONTENT

Supporting Information

The Supporting Information is available free of charge at https://pubs.acs.org/doi/10.1021/acs.molpharmaceut.1c00918.

Further details about the preparation of polymeric micelles in Table S1; data regarding polymer characterization using ^{1}H NMR, DOSY NMR, and SEC in Figures S1 and S2, Figure S3, and Table S2, respectively; micellar morphology assessed by TEM (Figure S4); additional results related to the *in silico* EGFR binding analysis shown comparing GE11 and EGF ligands (Figure S5); *in vitro* cell uptake studies supplemented by flow cytometry dot-plot graphs (Figure S6) and confocal microscopy images (Figure S7); EGFR expression among the CRC cells used in the studies that was relatively quantified by Western blot (Figure S8); safety profile of empty polymeric micelles on HCT116 PTEN$^{-/-}$ cells in Figure S9; correlation between accumulation of polymeric micelles and incidence of metastasis among the main organs assessed by *ex vivo* optical imaging (Figure S10) (PDF)

■ AUTHOR INFORMATION

Corresponding Author

Afsaneh Lavasanifar − *Faculty of Pharmacy and Pharmaceutical Sciences, University of Alberta, Edmonton, AB T6G 2EZ, Canada; Department of Chemical and Materials Engineering, Faculty of Engineering, University of Alberta, Edmonton, AB T6G 2H5, Canada;* orcid.org/0000-0001-5108-7124; Phone: (780) 492-2742; Email: afsaneh@ualberta.ca

Authors

Igor Moura de Paiva − *Faculty of Pharmacy and Pharmaceutical Sciences, University of Alberta, Edmonton, AB T6G 2EZ, Canada;* orcid.org/0000-0002-2077-0016

Mohammad Reza Vakili − *Faculty of Pharmacy and Pharmaceutical Sciences, University of Alberta, Edmonton, AB T6G 2EZ, Canada*

Amir Hasan Soleimani − *Faculty of Pharmacy and Pharmaceutical Sciences, University of Alberta, Edmonton, AB T6G 2EZ, Canada*

Seyed Amirhossein Tabatabaei Dakhili − *Faculty of Pharmacy and Pharmaceutical Sciences, University of Alberta, Edmonton, AB T6G 2EZ, Canada;* orcid.org/0000-0002-8104-5029

Sirazum Munira − *Faculty of Pharmacy and Pharmaceutical Sciences, University of Alberta, Edmonton, AB T6G 2EZ, Canada*

https://doi.org/10.1021/acs.molpharmaceut.1c00918
Mol. Pharmaceutics 2022, 19, 1825−1838

Marco Paladino − *Department of Chemistry, Faculty of Science, University of Alberta, Edmonton, AB T6G 2G2, Canada*

Gary Martin − *Department of Biochemistry and Molecular Biology, University of Calgary, Calgary, AB T2N 4Z6, Canada*

Frank R. Jirik − *Department of Biochemistry and Molecular Biology and Department of Medicine, University of Calgary, Calgary, AB T2N 4Z6, Canada*

Dennis G. Hall − *Department of Chemistry, Faculty of Science, University of Alberta, Edmonton, AB T6G 2G2, Canada;* orcid.org/0000-0001-8555-6400

Michael Weinfeld − *Department of Oncology, Faculty of Medicine and Dentistry, University of Alberta, Edmonton, AB T6G 1Z2, Canada;* orcid.org/0000-0002-8773-1425

Complete contact information is available at: https://pubs.acs.org/10.1021/acs.molpharmaceut.1c00918

Notes

The authors declare the following competing financial interest(s): Material in this manuscript has been included in recent U.S. patent applications. Dr. Lavasanifar is Vice-President of Meros Polymers which has the license to the PEO-PBCL polymer used in this manuscript.

■ ACKNOWLEDGMENTS

This work was supported by grants funded by the Canadian Institutes of Health Research (Grant PJT168869) to M.W. and (Grants MOP 159757 and MOP 178028) to A.L. and the Alberta Cancer Foundation Transformative Program Project (Grant 26603) to D.H., F.J., A.L., and M.W. The authors thanks Sams Sadat and Zahra Shire for their technical assistance.

■ REFERENCES

(1) Wu, K.; Zhai, M. Z.; Weltzien, E. K.; Cespedes Feliciano, E. M.; Meyerhardt, J. A.; Giovannucci, E.; Caan, B. J. Non-alcoholic fatty liver disease and colorectal cancer survival. *Cancer Causes Control* **2019**, *30*, 165−168.

(2) Biller, L. H.; Schrag, D. Diagnosis and Treatment of Metastatic Colorectal Cancer: A Review. *J. Am. Med. Assoc.* **2021**, *325*, 669−685.

(3) Smith, A. J.; Driman, D. K.; Spithoff, K.; Hunter, A.; McLeod, R. S.; Simunovic, M.; Langer, B. Guideline for optimization of colorectal cancer surgery and pathology. *J. Surg. Oncol.* **2010**, *101*, 5−12.

(4) Ji, X.; Zhao, Y.; Zhu, X.; Shen, Z.; Li, A.; Chen, C.; Chu, X. Outcomes of Stereotactic Body Radiotherapy for Metastatic Colorectal Cancer With Oligometastases, Oligoprogression, or Local Control of Dominant Tumors. *Front. Oncol.* **2021**, *10*, 595781.

(5) Valderrama-Treviño, A. I.; Barrera-Mera, B.; Montalvo-Javé, E. E.; Ceballos-Villalva, J. C. Hepatic Metastasis from Colorectal Cancer. *Euroasian J. Hepatogastroenterology* **2017**, *7*, 166−175.

(6) Pabla, B.; Bissonnette, M.; Konda, V. J. Colon cancer and the epidermal growth factor receptor: Current treatment paradigms, the importance of diet, and the role of chemoprevention. *World J. Clin. Oncol.* **2015**, *6*, 133−141.

(7) Siddiqui, A. D.; Piperdi, B. KRAS Mutation in Colon Cancer: A Marker of Resistance to EGFR-I Therapy. *Ann. Surg. Oncol.* **2010**, *17*, 1168−1176.

(8) Troiani, T.; Martinelli, E.; Napolitano, S.; Vitagliano, D.; Ciuffreda, L. P.; Costantino, S.; Morgillo, F.; Capasso, A.; Sforza, V.; Nappi, A.; De Palma, R.; D'Aiuto, E.; Berrino, L.; Bianco, R.; Ciardiello, F. Increased TGF-α as a Mechanism of Acquired Resistance to the Anti-EGFR Inhibitor Cetuximab through EGFR-MET Interaction and Activation of MET Signaling in Colon Cancer Cells. *Clin. Cancer Res.* **2013**, *19*, 6751−6765.

(9) Edwards, M. S.; Chadda, S. D.; Zhao, Z.; Barber, B. L.; Sykes, D. P. A systematic review of treatment guidelines for metastatic colorectal cancer. *Colorectal Dis* **2012**, *14*, e31−e47.

(10) Kuipers, E. J.; Grady, W. M.; Lieberman, D.; Seufferlein, T.; Sung, J. J.; Boelens, P. G.; van de Velde, C. J. H.; Watanabe, T. Colorectal Cancer. *Nat. Rev. Dis. Primers* **2015**, *1*, 15065.

(11) Reilly, N. M.; Novara, L.; Di Nicolantonio, F.; Bardelli, A. Exploiting DNA repair defects in colorectal cancer. *Mol. Oncol.* **2019**, *13*, 681−700.

(12) Mauri, G.; Arena, S.; Siena, S.; Bardelli, A.; Sartore-Bianchi, A. The DNA damage response pathway as a land of therapeutic opportunities for colorectal cancer. *Ann. Oncol.* **2020**, *31*, 1135−1147.

(13) Shire, Z.; Vakili, M. R.; Morgan, T. D. R.; Hall, D. G.; Lavasanifar, A.; Weinfeld, M. Nanoencapsulation of Novel Inhibitors of PNKP for Selective Sensitization to Ionizing Radiation and Irinotecan and Induction of Synthetic Lethality. *Mol. Pharmaceutics* **2018**, *15*, 2316−2326.

(14) Mereniuk, T. R.; Maranchuk, R. A.; Schindler, A.; Penner-Chea, J.; Freschauf, G. K.; Hegazy, S.; Lai, R.; Foley, E.; Weinfeld, M. Genetic Screening for Synthetic Lethal Partners of Polynucleotide Kinase/Phosphatase: Potential for Targeting SHP-1-Depleted Cancers. *Cancer Res.* **2012**, *72*, 5934−5944.

(15) Freschauf, G. K.; Karimi-Busheri, F.; Ulaczyk-Lesanko, A.; Mereniuk, T. R.; Ahrens, A.; Koshy, J. M.; Rasouli-Nia, A.; Pasarj, P.; Holmes, C. F. B.; Rininsland, F.; Hall, D. G.; Weinfeld, M. Identification of a Small Molecule Inhibitor of the Human DNA Repair Enzyme Polynucleotide Kinase/Phosphatase. *Cancer Res.* **2009**, *69*, 7739−7746.

(16) Sadat, S.; Paiva, I. M.; Shire, Z.; Sanaee, F.; Morgan, T. D. R.; Paladino, M.; Karimi-Busheri, F.; Mani, R. S.; Martin, G. R.; Jirik, F. R.; Hall, D. G.; Weinfeld, M.; Lavasanifar, A. A synthetically lethal nanomedicine delivering novel inhibitors of polynucleotide kinase 3′-phosphatase (PNKP) for targeted therapy of PTEN-deficient colorectal cancer. *J. Controlled Release* **2021**, *334*, 335−352.

(17) Sadat, S. M. A.; Wuest, M.; Paiva, I. M.; Munira, S.; Sarrami, N.; Sanaee, F.; Yang, X.; Paladino, M.; Binkhathlan, Z.; Karimi-Busheri, F.; Martin, G. R.; Jirik, F. R.; Murray, D.; Gamper, A. M.; Hall, D. G.; Weinfeld, M.; Lavasanifar, A. Nano-delivery of a novel inhibitor of polynucleotide kinase/phosphatase (PNKP) for targeted sensitization of colorectal cancer to radiation-induced DNA damage. *Front. Oncol.* **2021**, *11*, 772920.

(18) Paiva, I.; Mattingly, S.; Wuest, M.; Leier, S.; Vakili, M. R.; Weinfeld, M.; Lavasanifar, A.; Wuest, F. Synthesis and Analysis of 64Cu-Labeled GE11-Modified Polymeric Micellar Nanoparticles for EGFR-Targeted Molecular Imaging in a Colorectal Cancer Model. *Mol. Pharmaceutics* **2020**, *17*, 1470−1481.

(19) Genta, I.; Chiesa, E.; Colzani, B.; Modena, T.; Conti, B.; Dorati, R. GE11 Peptide as an Active Targeting Agent in Antitumor Therapy: A Minireview. *Pharmaceutics* **2018**, *10*, No. E2.

(20) Langer, R. Drug Delivery and Targeting. *Nature* **1998**, *392*, 5−10.

(21) Tebbutt, N.; Pedersen, M. W.; Johns, T. G. Targeting the ERBB family in cancer: couples therapy. *Nat. Rev. Cancer* **2013**, *13*, 663−673.

(22) Ono, M.; Kuwano, M. Molecular Mechanisms of Epidermal Growth Factor Receptor (EGFR) Activation and Response to Gefitinib and Other EGFR-Targeting Drugs. *Clin. Cancer Res.* **2006**, *12*, 7242−7251.

(23) Li, Z.; Zhao, R.; Wu, X.; Sun, Y.; Yao, M.; Li, J.; Xu, Y.; Gu, J. Identification and characterization of a novel peptide ligand of epidermal growth factor receptor for targeted delivery of therapeutics. *FASEB J.* **2005**, *19*, 1978−1985.

(24) Gil, D.; Schrum, A. G. Strategies to stabilize compact folding and minimize aggregation of antibody-based fragments. *Adv. Biosci. Biotechnol.* **2013**, *4*, 73−84.

(25) Hossein-Nejad-Ariani, H.; Althagafi, E.; Kaur, K. Small Peptide Ligands for Targeting EGFR in Triple Negative Breast Cancer Cells. *Sci. Rep.* **2019**, *9*, 2723.

(26) Vlieghe, P.; Lisowski, V.; Martinez, J.; Khrestchatisky, M. Synthetic therapeutic peptides: science and market. *Drug Discovery Today* **2010**, *15*, 40−56.
(27) Mickler, F. M.; Möckl, L.; Ruthardt, N.; Ogris, M.; Wagner, E.; Bräuchle, C. Tuning Nanoparticle Uptake: Live-Cell Imaging Reveals Two Distinct Endocytosis Mechanisms Mediated by Natural and Artificial EGFR Targeting Ligand. *Nano Lett.* **2012**, *12*, 3417−3423.
(28) Truebenbach, I.; Zhang, W.; Wang, Y.; Kern, S.; Höhn, M.; Reinhard, S.; Gorges, J.; Kazmaier, U.; Wagner, E. Co-delivery of pretubulysin and siEG5 to EGFR overexpressing carcinoma cells. *Int. J. Pharm.* **2019**, *569*, 118570.
(29) Mondal, G.; Kumar, V.; Shukla, S. K.; Singh, P. K.; Mahato, R. I. EGFR-Targeted Polymeric Mixed Micelles Carrying Gemcitabine for Treating Pancreatic Cancer. *Biomacromolecules* **2016**, *17*, 301−313.
(30) Zou, Y.; Xia, Y.; Meng, F.; Zhang, J.; Zhong, Z. GE11-Directed Functional Polymersomal Doxorubicin as an Advanced Alternative to Clinical Liposomal Formulation for Ovarian Cancer Treatment. *Mol. Pharmaceutics* **2018**, *15*, 3664−3671.
(31) Chu, W.-Y.; Tsai, M.-H.; Peng, C.-L.; Shih, Y.-H.; Luo, T.-Y.; Yang, S.-J.; Shieh, M.-J. pH-Responsive Nanophotosensitizer for an Enhanced Photodynamic Therapy of Colorectal Cancer Over-expressing EGFR. *Mol. Pharmaceutics* **2018**, *15*, 1432−1444.
(32) Garg, S. M.; Xiong, X.-B.; Lu, C.; Lavasanifar, A. Application of Click Chemistry in the Preparation of Poly(ethylene oxide)-*block*-poly(ε-caprolactone) with Hydrolyzable Cross-Links in the Micellar Core. *Macromolecules* **2011**, *44*, 2058−2066.
(33) Mahmud, A.; Xiong, X.-B.; Lavasanifar, A. Novel Self-Associating Poly(ethylene oxide)-*block*-poly(ε-caprolactone) Block Copolymers with Functional Side Groups on the Polyester Block for Drug Delivery. *Macromolecules* **2006**, *39*, 9419−9428.
(34) Nagasaki, Y.; Kutsuna, T.; Iijima, M.; Kato, M.; Kataoka, K.; Kitano, S.; Kadoma, Y. Formyl-Ended Heterobifunctional Poly(ethylene oxide): Synthesis of Poly(ethylene oxide) with a Formyl Group at One End and a Hydroxyl Group at the Other End. *Bioconjugate Chem.* **1995**, *6*, 231−233.
(35) Xiong, X.-B.; Lavasanifar, A. Traceable Multifunctional Micellar Nanocarriers for Cancer-Targeted Co-delivery of MDR-1 siRNA and Doxorubicin. *ACS Nano* **2011**, *5*, 5202−5213.
(36) Garg, S. M.; Paiva, I. M.; Vakili, M. R.; Soudy, R.; Agopsowicz, K.; Soleimani, A. H.; Hitt, M.; Kaur, K.; Lavasanifar, A. Traceable PEO-poly(ester) micelles for breast cancer targeting: The effect of core structure and targeting peptide on micellar tumor accumulation. *Biomaterials* **2017**, *144*, 17−29.
(37) Topel, Ö.; Çakır, B. A.; Budama, L.; Hoda, N. Determination of critical micelle concentration of polybutadiene-*block*-poly(ethyleneoxide) diblock copolymer by fluorescence spectroscopy and dynamic light scattering. *J. Mol. Liq.* **2013**, *177*, 40−43.
(38) Owen, S. C.; Chan, D. P. Y.; Shoichet, M. S. Polymeric micelle stability. *Nano Today* **2012**, *7*, 53−65.
(39) Ferguson, K. M.; Berger, M. B.; Mendrola, J. M.; Cho, H.-S.; Leahy, D. J.; Lemmon, M. A. EGF Activates Its Receptor by Removing Interactions that Autoinhibit Ectodomain Dimerization. *Mol. Cell* **2003**, *11*, 507−517.
(40) Pettersen, E. F.; Goddard, T. D.; Huang, C. C.; Couch, G. S.; Greenblatt, D. M.; Meng, E. C.; Ferrin, T. E. UCSF Chimera—A visualization system for exploratory research and analysis. *J. Comput. Chem.* **2004**, *25*, 1605−1612.
(41) Morris, G. M.; Huey, R.; Lindstrom, W.; Sanner, M. F.; Belew, R. K.; Goodsell, D. S.; Olson, A. J. AutoDock4 and AutoDockTools4: Automated docking with selective receptor flexibility. *J. Comput. Chem.* **2009**, *30*, 2785−2791.
(42) Trott, O.; Olson, A. J. AutoDock Vina: Improving the speed and accuracy of docking with a new scoring function, efficient optimization, and multithreading. *J. Comput. Chem.* **2010**, *31*, 455−461.
(43) Sousa da Silva, A. W.; Vranken, W. F. ACPYPE - AnteChamber PYthon Parser interfacE. *BMC Res. Notes* **2012**, *5*, 367.
(44) Abraham, M. J.; Murtola, T.; Schulz, R.; Páll, S.; Smith, J. C.; Hess, B.; Lindahl, E. GROMACS: High performance molecular simulations through multi-level parallelism from laptops to supercomputers. *SoftwareX* **2015**, *1*−*2*, 19−25.
(45) Kumari, R.; Kumar, R.; Open Source Drug Discovery Consortium; Lynn, A. g_*mmpbsa*—A GROMACS Tool for High-Throughput MM-PBSA Calculations. *J. Chem. Inf. Model.* **2014**, *54*, 1951−1962.
(46) Bondareva, A.; Downey, C. M.; Ayres, F.; Liu, W.; Boyd, S. K.; Hallgrimsson, B.; Jirik, F. R. The Lysyl Oxidase Inhibitor, β-Aminopropionitrile, Diminishes the Metastatic Colonization Potential of Circulating Breast Cancer Cells. *PLoS One* **2009**, *4*, No. e5620.
(47) Lee, C.; Kim, J.-S.; Waldman, T. *PTEN* Gene Targeting Reveals a Radiation-Induced Size Checkpoint in Human Cancer Cells. *Cancer Res.* **2004**, *64*, 6906−6914.
(48) Tseng, W.; Leong, X.; Engleman, E. Orthotopic Mouse Model of Colorectal Cancer. *J. Visualized Exp.* **2007**, *10*, 484−488.
(49) Zhou, X. X.; Jin, L.; Qi, R. Q.; Ma, T. pH-responsive polymeric micelles self-assembled from amphiphilic copolymer modified with lipid used as doxorubicin delivery carriers. *R. Soc. Open Sci.* **2018**, *5*, 171654.
(50) Doncom, K. E. B.; Pitto-Barry, A.; Willcock, H.; Lu, A.; McKenzie, B. E.; Kirby, N.; O'Reilly, R. K. Complementary light scattering and synchrotron small-angle X-ray scattering studies of the micelle-to-unimer transition of polysulfobetaines. *Soft Matter* **2015**, *11*, 3666−76.
(51) He, H.; Ren, Y.; Wang, Z.; Xie, Z. A pH-responsive poly(ether amine) micelle with hollow structure for controllable drug release. *RSC Adv.* **2016**, *6*, 91940−46.
(52) Céspedes, M. V.; Espina, C.; García-Cabezas, M. A.; Trias, M.; Boluda, A.; Gómez del Pulgar, M. T.; Sancho, F. J.; Nistal, M.; Lacal, J. C.; Mangues, R. Orthotopic Microinjection of Human Colon Cancer Cells in Nude Mice Induces Tumor Foci in All Clinically Relevant Metastatic Sites. *Am. J. Pathol.* **2007**, *170*, 1077−1085.
(53) Rapic, S.; Vangestel, C.; Verhaeghe, J.; Van den Wyngaert, T.; Hinz, R.; Verhoye, M.; Pauwels, P.; Staelens, S.; Stroobants, S. Characterization of an Orthotopic Colorectal Cancer Mouse Model and Its Feasibility for Accurate Quantification in Positron Emission Tomography. *Mol. Imaging Biol.* **2017**, *19*, 762−771.
(54) Kuo, W.-T.; Lin, W.-C.; Chang, K.-C.; Huang, J.-Y.; Yen, K.-C.; Young, I.-C.; Sun, Y.-J.; Lin, F.-H. Quantitative Analysis of Ligand-EGFR Interactions: A Platform for Screening Targeting Molecules. *PLoS One* **2015**, *10*, No. e0116610.
(55) Ongarora, B. G.; Fontenot, K. R.; Hu, X.; Sehgal, I.; Satyanarayana-Jois, S. D.; Vicente, M. G. H. Phthalocyanine−Peptide Conjugates for Epidermal Growth Factor Receptor Targeting. *J. Med. Chem.* **2012**, *55*, 3725−3738.
(56) Hanahan, D.; Weinberg, R. A. Hallmarks of Cancer: The Next Generation. *Cell* **2011**, *144*, 646−674.
(57) Zarschler, K.; Prapainop, K.; Mahon, E.; Rocks, L.; Bramini, M.; Kelly, P. M.; Stephan, H.; Dawson, K. A. Diagnostic nanoparticle targeting of the EGF-receptor in complex biological conditions using single-domain antibodies. *Nanoscale* **2014**, *6*, 6046−6056.
(58) Danhier, F.; Le Breton, A.; Préat, V. RGD-Based Strategies To Target Alpha(v) Beta(3) Integrin in Cancer Therapy and Diagnosis. *Mol. Pharmaceutics* **2012**, *9*, 2961−2973.
(59) Raghuwanshi, Y.; Etayash, H.; Soudy, R.; Paiva, I.; Lavasanifar, A.; Kaur, K. Proteolytically Stable Cyclic Decapeptide for Breast Cancer Cell Targeting. *J. Med. Chem.* **2017**, *60*, 4893−4903.

https://doi.org/10.1021/acs.molpharmaceut.1c00918
Mol. Pharmaceutics 2022, 19, 1825−1838